Title

Boosting the sodium storage behaviors of carbon materials in ether-based electrolyte through the artificial manipulation of microstructure

Authors

Xiao, Wei
Sun, Qian
Liu, Jian
et al.

Publication Date

2019-12-01

DOI

10.1016/j.nanoen.2019.104177

Peer reviewed

Boosting the sodium storage behaviors of carbon materials in ether-based electrolyte through the artificial manipulation of microstructure

Wei Xiao[1,2,4], Qian Sun[1], Jian Liu[1,3], Biwei Xiao[1],Yulong Liu[1], Per-Anders Glans[3], Jun Li[2], Ruying Li[1], Xifei Li[4,5],Jinghua Guo[3], Wanli Yang[3], Tsun-Kong Sham[2*], Xueliang Sun[1*]

1. Department of Mechanical & Materials Engineering, University of Western Ontario, London, Ontario, Canada
2. Department of Chemistry, University of Western Ontario, London, Ontario, Canada
3. Advanced Light Source, Lawrence Berkeley National Laboratory, Berkeley, California, United States
4. Institute of Advanced Electrochemical Energy, School of Materials Science and Engineering, Xi'an University of Technology, Xi'an, Shaanxi, 710048, China
5. State Center for International Cooperation on Designer Low-carbon & Environmental Materials (CDLCEM), Zhengzhou University, Zhengzhou, Henan, 450001, China

Abstract: The porous carbon blacks rationally designed by an NH_3 etching route have been investigated as anode materials in DEGDME (Diethylene glycol dimethyl ether)-based electrolyte for sodium-ion batteries. The as-synthesized CBN35 carbon black with highest microporosity and appropriate surface area, exhibits a large specific charge capacity of 352 mAh g^{-1} at 50 mA g^{-1} and a superior rate capability of 125 mAh g^{-1} at 3200 mA g^{-1}. Even cycled at 1600 mA g^{-1} over 3200 cycles, an outstanding reversible capacity of 103 mAh g^{-1} with a negligible 0.0162% capacity loss per cycle can still be achieved. Based on multimodal characterizations, including the structural probe of the evolution of carbon materials, the electrochemical techniques, and surface-sensitive XAS measurements, the exceptional electrochemical properties stem from several advantages of the modified carbon black system. The particular microporous structure provides relatively more accessible sodium storage sites and a hybrid insertion mechanism with sodium ion insertion into disordered structure while solvated sodium ion intercalation into graphitic phase. The system also features a controlled emergence of a robust SEI thin film, which could maintain the fragile porous structure and facilitate the sodium ions/solvated sodium ion migration.

Key words: sodium-ion batteries; anode; porous carbon; microporosity; ether-based electrolyte; cointercalation

1. Introduction

The commercialization of lithium-ion batteries has stimulated the development of portable electronics and recently envisioned its feasibility for powering electric vehicles[1-3]. However, the huge potential demand for geologically limited lithium resource along with soaring prices in recent decades, has propelled the pursuit of sustainable energy storage systems with low cost and high reliability[4-6]. Sodium-ion batteries, owing to its abundant element reserve with widespread natural distribution and appropriate redox potential ($E_{Na^+/Na}$= -2.71 V vs. S. H. E) as well as analogous reaction mechanism to its lithium counterparts, have been extensively studied as promising alternatives for lithium-ion batteries in recent years, particularly in the market of large-scale grid energy storage[7-9]. However, the increased atomic weight of sodium ions and higher redox potential for Na^+/Na couple may unavoidably lower the theoretical energy density of sodium-ion batteries[10,11]. More seriously, the inherent larger ionic size of sodium ions, compared with lithium (1.02 vs 0.76 Å), further triggers the kinetics challenges involving sluggish sodium ion diffusion, and host structural stability issue concerning the large volume change during sodiation/desodiation process. Additionally, the complex sodium ion chemistry regarding interactions between cations and host structure as well as subsequent SEI (solid electrolyte interphase) formation also lead to the instability of electrochemical properties[8,12]. It is therefore urgent to develop advanced electrode materials with more accessible sodium storage sites and higher physiochemical stability to enable the sustainability of high-performance sodium ion batteries.

Generally, it is problematic to directly apply sodium metal as anode materials in sodium ion batteries, due to safety hazard resulted from its low meting point and internal short circuits after dendrite formation[5]. Compare with the conventional graphite with in-plane long range order and stacking order, which can reversibly intercalate lithium ions in formation of various graphite intercalation compounds(GICs), disordered carbon materials, with larger interlayer distance stemmed from irregular structures comprising curved graphene nanosheets and turbostratic graphitic nanodomains, can effectively accommodate the insertion/extraction process of sodium ions with larger ionic size[13-15]. Admittedly, typical hard carbon and related materials can deliver a reversible capacity around 300 mAh g^{-1}; but the rate performance and cycle stability for these materials are still poor[16-24]. Well-established nanotechnologies in lithium ion batteries have been introduced into sodium systems in preparation of carbonaceous materials with expanded interlayer distance for buffering the huge structural strain from sodiation/desodiation process ,

increasing the contact area between electrode and electrolyte for excellent rate capability, and further shortening the path lengths for electronic transport and sodium ions diffusion[25,26]. Previous research has demonstrated the use of templated carbon with hierarchical porosity as an anode material displaying excellent rate performance[27]. Joachim Maier et al[28] further synthesized hollow carbon nanospheres by hydrothermal method with subsequent annealing and obtain a reversible capacity of 50 mAh g^{-1} at 10 A g^{-1} ,while similar hollow carbon nanowires[29] and ultrathin hollow carbon nanospheres[30] can both deliver a larger reversible capacity with extended cycle life. Notably, the nanostructure design ranging from 1D carbon nanofibers[31-35]/microtubes[36], 2D graphene[37-39]/carbon nanosheets[40], to 3D carbon frameworks[41-43] and hard carbon matrix[44], have been successfully exemplified in promoting the electrochemical performance of carbon-based materials. For example, Xiulei Ji et al[34] derived carbon nanofibers from cellulose nanofibers with an excellent rate performance of 85 mAh g^{-1} at 2 A g^{-1} as well as a superior cycling stability of 176 mA h g^{-1} at 200 mA g^{-1} over 600 cycles. And a free-standing and binder-free carbon nanofibers electrode obtained from pyrolysis of PAN-F127/DMF nanofibers through an electrospinning method could even deliver an reversible capacity of ~140 mAh g^{-1} after 1000 cycles at 0.5 A g^{-1} [33]. Moreover, the porous carbon frameworks synthesized from carbon quantum dots could present remarkable cycle life over 10000 cycles with a highly reversible capacity of 137 mAh g^{-1} at 5 A g^{-1} [42]. In parallel with these developments, much efforts have been devoted to tailor carbon materials by heteroatom doping for improved conductivity and extra defective sites for sodium ion storage, such as nitrogen doping[45-51], sulfur doping[40,52-54], fluorine doping[55], hydrogen-doping[56], and POx doping[57], while biomass-derived carbon materials could also demonstrate its high sodium storage capability for unique porous structure with high disordered degree[22,24,58-61]. Particularly, the sulfur-doped disordered carbon prepared from carbonizing the mixture of NTCDA and sulfur, could present a ultra-high reversible capacity of 271 mAh g^{-1} at 1 A g^{-1} over 1000 cycles[52].

Recently, graphite was firstly revisited by Philipp Adelhelm et al in diglyme-based electrolyte with a reversible capacity of 100 mAh g^{-1} over 1000 cycles[62], while Kisuk Kang et al further optimized the electrode performance with a stable specific capacity of 150 mAh g^{-1} for 2500 cycles[63] and proposed the formation of solvated sodium ion species as well as its thermodynamically favorable intercalation process[64]. Later, Quanhong Yang et al, applied the high specific surface area carbon in ether-based electrolyte and achieve a large reversible

capacity of 509 mAh g^{-1} at 100 mA $g^{-1}$with the desirable stability up to 1000 cycles at 1.0 A g^{-1}.[65]

Importantly, DEGDME-based electrolyte was successfully applied for a commercial non-porous carbon black with significantly improved reversible capacity and cycle stability. This is achieved by taking advantage of sodium insertion into disordered structure and sodium ion-solvent cointercalation into graphitic structure. However, the present accessible capacity is still low when compared with conventional hard carbon based materials. Therefore, the rational design of electrode materials with more active sodium storage sites is urgently necessary.

Herein, we develop a facile method to tailor the porosity of carbon black, which is introduced into an ether-based electrolyte system for the first time. By incorporating different sodation/desodiation avenues, we show that the optimized porous structure with minor heteroatom doping could enable the highly stable capacity with ultra-long cycle life as well as remarkable rate performance.

2. Experimental

2.1 Materials preparation

Commercial N330 carbon was used in all experiments as the pristine material. And based on our previous research[66], NH_3 gas was introduced at 1050 °C to etch the N330 carbon black yielding porous carbon with desired mass loss. Typically, 500 mg of N330 powder in a fused silica boat was pyrolyzed in a fused silica reactor under NH_3 at 1050 °C until the desired mass loss achieved. Samples with mass loss of 10%, 35%, 54%, were referred as CBN10, CBN35, and CBN54, respectively.

Sodium triflate ($NaCF_3SO_3$, 98%, Sigma Aldrich) and molecular sieves (4 Å, Sigma Aldrich) were firstly dried at 150 °C in a vacuum oven for 2 days while molecular sieves were later employed to remove the residual water in solvents. And two kinds of electrolytes were carefully synthesized in a argon-filled glove box by dissolving 1.0 M sodium triflate ($NaCF_3SO_3$, 98%, Sigma Aldrich) into DEGDME (98.9%, Sigma Aldrich) and EC/DEC with 1:1 in volume ratio(Sigma Aldrich), respectively.

2.2 Physical characterizations

The crystalline structure of carbon materials was studied using X-ray Diffraction (XRD) by a Bruker D8Advance (Cu-Kα source, 40kV, 40mA) spectrometer while Raman scattering spectra were recorded using a HORIBA Scientific LabRAM HR Raman spectrometer system equipped with a 532.4 nm laser. A Folio Micromeritics Tristar II surface area analyzer was employed to measure N_2 adsorption/desorption isotherm and pore size distribution. Morphology was observed using Hitachi S-4800 field emission scanning electron microscope (FE-SEM) operated at 5 keV and high-resolution transmission electron microscopy (HRTEM) (JEOL 2010 FEG). Synchrotron C K-edge X-ray absorption spectroscopy (XAS) measurements were conducted in Beamline 6.3.1.2 and 8.0.1.4 of Advanced Light Source in Lawrence Berkeley National Laboratory and The C 1s X-ray photoemission spectroscopies (XPS) were performed at the high resolution Spherical Grating Monochromator (SGM) beamline in Canadian Light Source (CLS). The excitation and pass energy for XPS are 700 and 500 eV, respectively.

2.3 Electrochemical measurement

Electrodes were prepared by casting the slurry, consisting of 80 wt.% active material, 10 wt.% acetylene black as the conductive agent, and 10 wt.% PVDF binder in suitable amount of N-methyl pyrrolidinone, onto copper foil. The casted foil was then vacuum dried at 80 °C for 12 h to remove residual water and excess NMP. And the electrodes were punched to ½ inch pellets which were further pressed and found to have a the loading mass of ~0.8 mg cm^{-2} Half-cell configuration 2032-type coin cells were fabricated in an Argon-filled glove box where sodium foils was used as an anode along with prepared N330 carbon electrodes and polypropylene membrane (Celgard 2400) as cathode and separator, respectively. Finally, the electrochemical properties were evaluated by cyclic voltammetry(CV) at 0.1 mV s^{-1} and electrochemical impedance spectra(EIS) at an AC voltage of 5 mV amplitude in the 100 kHz to 0.01 Hz frequency range in a Biologic VMP3 electrochemical station. The galvanostatic charge/discharge performances were examined between 0.001~2.5 V (vs Na/Na^+) at different current densities under room temperature using an Arbin BT-2000 Battery Tester.

3. Results and discussion

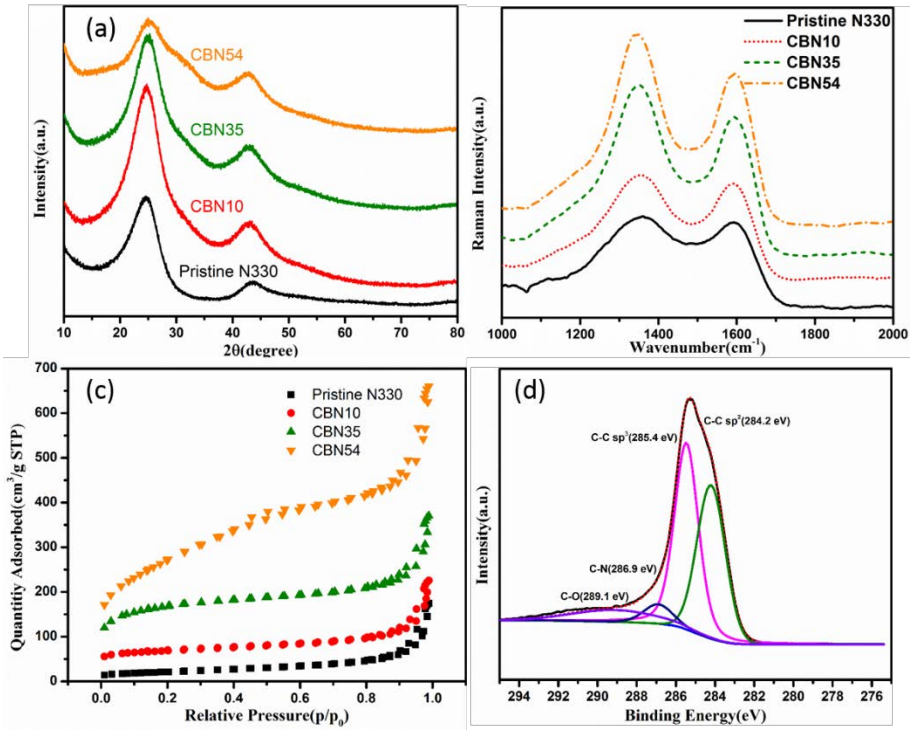

Fig.1 (a) X-ray diffraction patterns, (b) Raman spectra and (c) N_2 adsorption/desorption isotherm spectra for different carbon blacks. (d) Synchrotron C 1s X-ray photoelectron spectroscopy for CBN35 carbon black

X-ray diffraction was employed to understand the different microstructures of NH_3 etched porous carbon, as shown in Fig.1 (a). In all patterns, the obviously observed peaks at ~24 ° and ~42° could be indexed to (002) and (100) diffraction modes, related to the stacking order degree of graphitic carbon structure and the emergence of ordered hexagonal structure, respectively[30,67]. The (002) peak position would slightly move to low angle while its intensity firstly increases and then decreases along with the NH_3 etching process. Based on the classic Bragg equation and Scherrer equation[41,67,68], the interlayer distance (d_{002}), in-lane coherence length (L_c) and out-of-lane coherence length (L_a) for graphitic domains are calculated as listed in Table S1(supporting information). The apparent decrease of d_{002} as well as L_a and the increase of L_c from CBN10 to CBN54 carbon black clearly reflect the formation of short-range ordering and decomposition of disordered structure. However, during the initial etching process, , the L_a value increases while the L_c value decreases from N330 to CBN10 carbon black and maybe attributed to a particular formation mechanism previously investigated[69,70], involving the initial consumption of disordered carbon in the outmost surface part and following reactions between

NH_3 gas and amorphous carbon from the inner region as well as graphitic crystallite from remaining outside edges. Meanwhile, the D band for disordered phase and the G band for graphitic structure in Raman spectra, can be observed around 1343 and 1590 cm^{-1}, respectively. With the proceeding of NH_3 etching process, the corresponding D band would obviously sharpens with a decrease in the width at half maximum (FWHM), which further indicates the gradual diminishment of disordered phase and progressive formation of the ordered structure in carbon materials and agrees well with the results from XRD data as well as our previous report[66]. The unusual increase of I_D/I_G upon high-temperature NH_3 etching may be resulted from the curling of stacked graphitic layers and the subsequent shrinkage of small graphitic crystals in (100) directions[67,71]. Additionally, Fig.1(c) presents the nitrogen adsorption-desorption isotherms for different carbon blacks with pore size distributions are compared in Fig. S1. The introduction of reactive NH_3 gas effectively creates a porous structure with large surface area, ranging from 78 m^2 g^{-1} for pristine carbon black to 233, 583 and 783 m^2 g^{-1} for CBN10, CBN35 and CBN54 carbon materials, respectively. Among all samples, the CBN35 carbon black showed the highest specific surface area for microsporesThis type of architecture has been shown as the hosts for most active sites in Fe/N/C catalysts for oxygen reduction reaction at the cathode of proton exchange membrane (PEM) fuel cells[69,70]. As determined by our previous results from conventional XPS spectra[66], N atoms have been successfully doped into the etched porous carbon blacks but with quite limited content as listed in Table s1. Furthermore, CBN35 carbon black with a 1.4% N-doping content was further characterized by synchrotron-based C 1s XPS and this single broad peak could be deconvoluted into 4 separate peaks as shown in Fig.1 (d). Two broad peaks centered at 284.2 and 285.4 eV correspond to sp^2 and sp^3 hybridized carbon structures[72-74], respectively, while the comparatively weak peak at 286.9 eV is attributed to C-N bonds (N-sp^3 C configurations, sp^3-hybridized carbon atoms)[75-78]. And the appearance of C-O peak for –O-C=O- group at 289.1 eV[77-80] may be originated from immediate contact between etched carbon and air after pyrolysis, which conforms to our previous conventional XPS results[66]. The abundant experimental results from different characterization methods clearly demonstrate the structural evolution of carbon materials from solid spheres to microporous and mesoporous carbon. This structural morphology undoubtedly contributes to the improvements of sodium ion diffusion and intercalation performance of this anode material in sodium ion batteries.

Fig.2 depicts the morphology of different carbon materials. For pristine N330 carbon black as presented in Fig.2 (a), the nanoparticles with different sizes from 20 to 60 nm would severely agglomerate and unevenly distribute. Upon NH_3 etching, several tiny particles (<20 nm) and large particles (>40 nm) disappeared and the average particle size became relatively smaller as shown in Fig.2 (b-d), which is consistent with the results from our previous particle size distribution analysis[66]. Additionally, HRTEM images highlight the amorphous nature, and few-layer-stacked graphitic structure, with a interlayer distance of about 0.36 nm, of CBN35 (Fig.2(f)) and correlates well with data obtained from XRD.

On the basis of the well-understood NH_3 etching mechanism for N330 carbon black[54,55], Fig.3 further illustrates the carbon porosity formation process. Normally, the pristine N330 carbon particles consist of a graphitic structure and a disordered phase, but with almost no pore in the outside part. At the beginning of the etching process, the outer disordered carbon would firstly decompose under the etching reaction, generating several surface pores. With the gradual loss of the external disordered carbon, the as-resulted microspores would dimensionally grow deeper and larger, further leading to an increase of specific surface area of micropores and the eventual formation of mesopores. Following the complete consumption of outer disordered carbon, the NH_3 would not only react with the internal disordered part, but also begin to etching remaining graphitic structure on the outer surface. Eventually, the reduction of the outmost graphitic crystallite layer would inevitably result in decreased particle size.

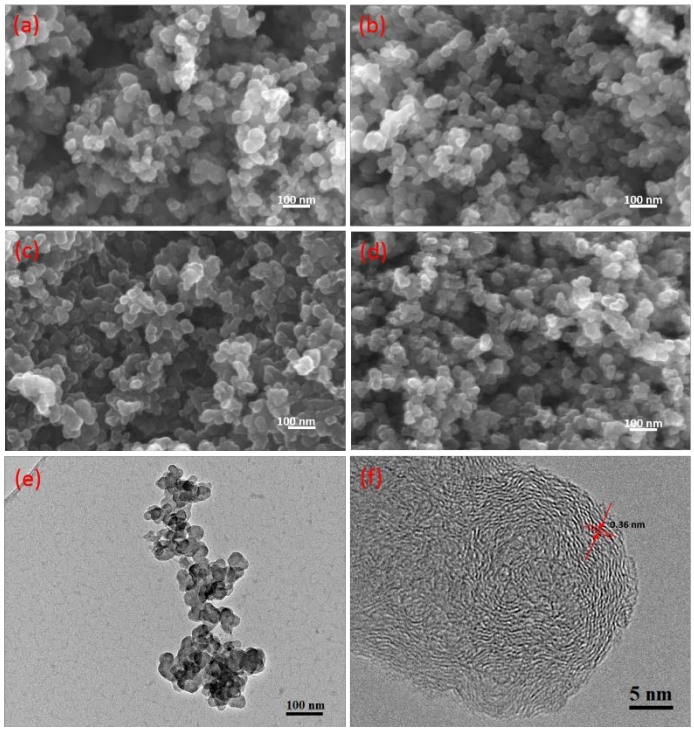

Fig.2 SEM images of (a) N330, (b) CBN10, (c) CBN35 and (d) CBN54 carbon blacks. (e)TEM image and (f) HRTEM image of CBN35 carbon black.

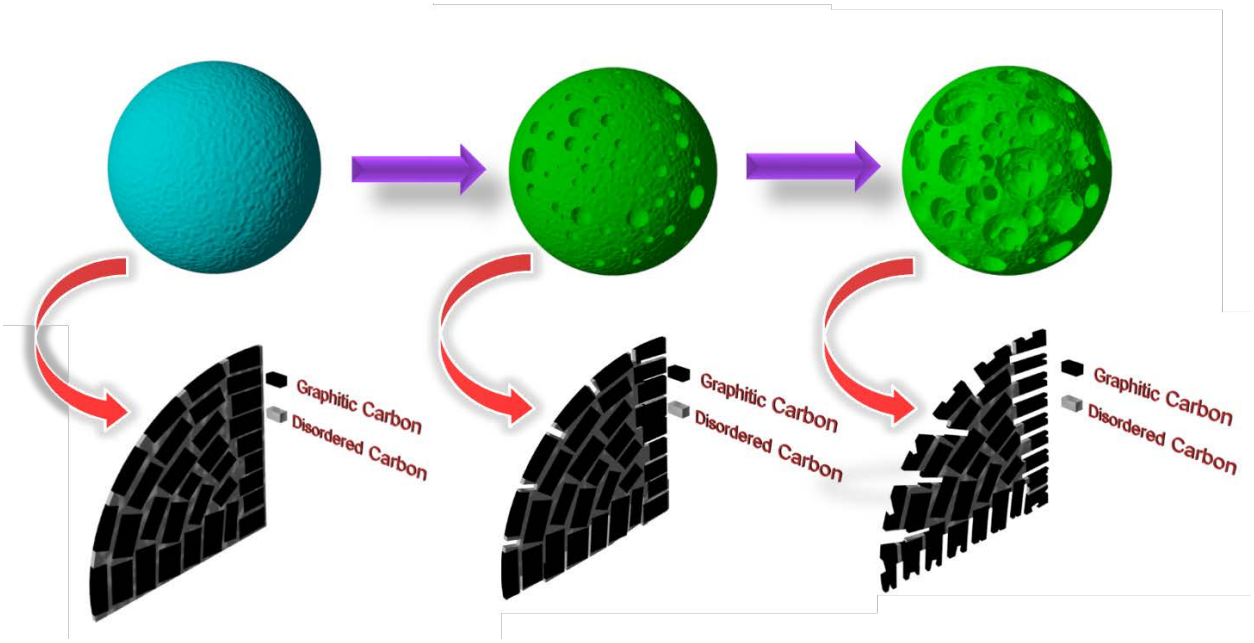

Fig. 3 Schematic diagram of carbon porosity formation during NH_3 etching process

Based on synergic mechanism of utilizing both disordered and graphitic structures for sodium storage, it's also critical to study the effects of porosity on electrochemical performance.

Surprisingly, the etched porous carbon blacks show very different sodium ion storage capabilities at different current densities as compared in Fig. 4. CBN35 carbon black exhibits an initial charge capacity of 352 mAh g^{-1} with the coulombic efficiency of 72.19% at a current density of 50 mA g^{-1}. As shown in Fig.4 (a), the subsequent discharging and charging curves scarcely move while most sodium intercalation/extraction processes efficiently occur below a voltage of 1.5 V, which is very desirable for coupling with existing cathode materials for full sodium ion batteries. Following 100 cycles of charging/discharging at 50 mA g^{-1}, CBN35 still maintains a highly reversible capacity of 336 mAh g^{-1} with 95.45% capacity retention as presented in Fig.4 (b). Conversely, pristine N330 displays an initial reversible of about 234 mAh g^{-1} with 84.12% capacity retention, and CBN 10 carbon black shows a noticeable capacity decay with a low reversible capacity of about 148 mA mAh g^{-1} and a 76.68% capacity retention. Additionally, the electrochemical properties of as-obtained porous carbon materials was further studied using extended cycling galvanostatic charging/discharging at elevated current densities. Comparatively, CBN35 is capable of achieving an initial reversible capacity of about 303 mAh g^{-1} with a coulombic efficiency of 70.79% at 100 mA g^{-1} while N330 and CBN10 only deliver an initial reversible capacity of 213 and 180 mAh g^{-1}, respectively. Different from the rapid capacity degradation for CBN10 with 58.89% capacity retention, CBN35 carbon retains a stable capacity of about 275 mAh g^{-1} with 90.76% capacity retention while N330 carbon has a capacity retention of 77.36% after 200 cycles at 100 mA g^{-1}, as depicted in Fig.4(c). Upon increasing the current density to 200 mA g^{-1}, CBN35 still delivers a high reversible capacity of 286 mAh g^{-1} with 69.59% coulombic efficiency in the first cycle. After 400 cycles, an exceptional reversible capacity of 229 mAh g^{-1} with 80.07% capacity retention is obtained, which is much higher than that of other carbon blacks tested herein. It is worth mentioning that CBN54 carbon black could present a low but stable reversible capacity of about 85 mAh g^{-1} at 50 mA g^{-1} without obvious voltage plateau as well as capacity loss when increasing current density, implying its limited active sites for efficient sodium ion storage, highly porous carbon structure for fast sodium ion diffusion after excessive NH3 etching treatment and capacitive behavior. Compared with the low reversible capacity and poor cycle stability obtained for CBN10, the outstanding electrochemical performance of CBN35 carbon is not only resulted from desirable creation of highest microporosity with suitable surface area and more active sodium ion storage sites, but also due to

the appropriate structural evolution of graphitic and disordered phases in noticeable heteroatom-doped carbon materials for enhancing the cointercalation in ether-based electrolyte.

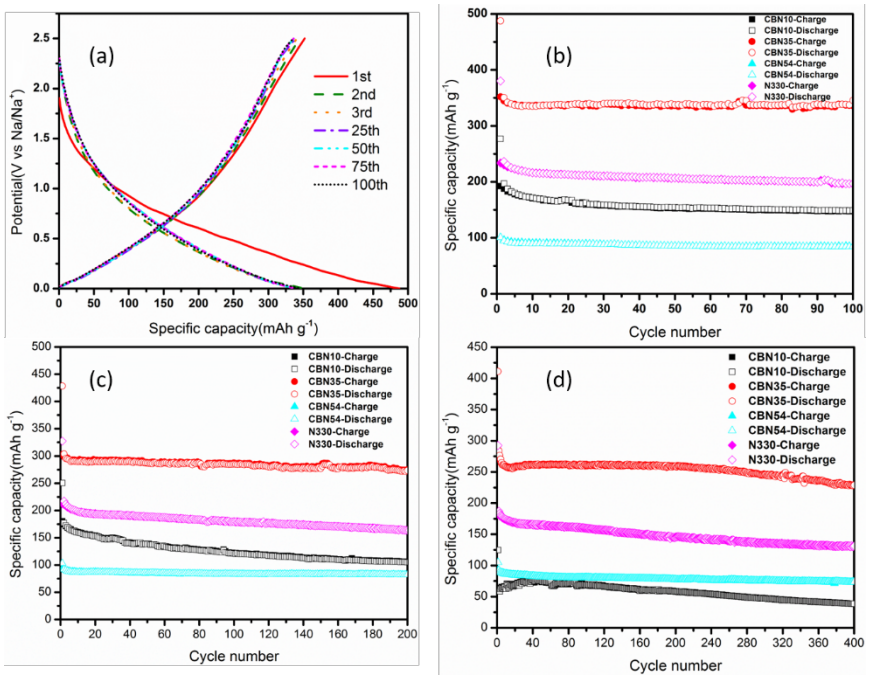

Fig. 4 (a) Discharge-charge profiles for CBN35 carbon black at a current density of 50 mA g^{-1}. Cycle performance of different carbon blacks at current densities of (a) 50, (b) 100 and (c) 200 mA g^{-1}.

The increased performance and long, stable cycle life seen for CBN35 is also verified in rate and cycle tests, as displayed in Fig. 5. CBN35 was capable of delivering a highly reversible capacity of 339, 290, 257, 211, 183 and 150 mAh g^{-1} at 50, 100, 200, 400, 800 and 1600 mA g^{-1}. Even when cycled at 3200 mA g^{-1}, a capacity of 125 mAh g^{-1} was found, demonstrating the versatile nature of this hierarchal porous structure. After decreasing the current density to 50 mA g^{-1}, the capacity could restore to 336 mAh g^{-1} with superior reversibility. And the cycling stability of CBN35 n was further evaluated at an ultrahigh current density of 1600 mA g^{-1}. Regardless of low initial coulombic efficiency of 77.38% and fast capacity degradation in first 100 cycles, the CBN35 carbon black could deliver an outstanding reversible capacity of 103 mAh g^{-1} over 3200 cycles with a negligible 0.0162% capacity loss per cycle, which is much better than electrochemical properties of carbon-based materials from most recentreports[22,36,53,56-58,61,67,81-88]. Importantly, the unique microporous structure allows for facile access to sodium ion storage sites, thereby allowing rapid reversible sodiation and desodiation process. Furthermore,

the porous nature of this material allows for a hybrid swift diffusion of sodium ions and solvated sodium ion species into the disordered and graphitic structure, respectively.

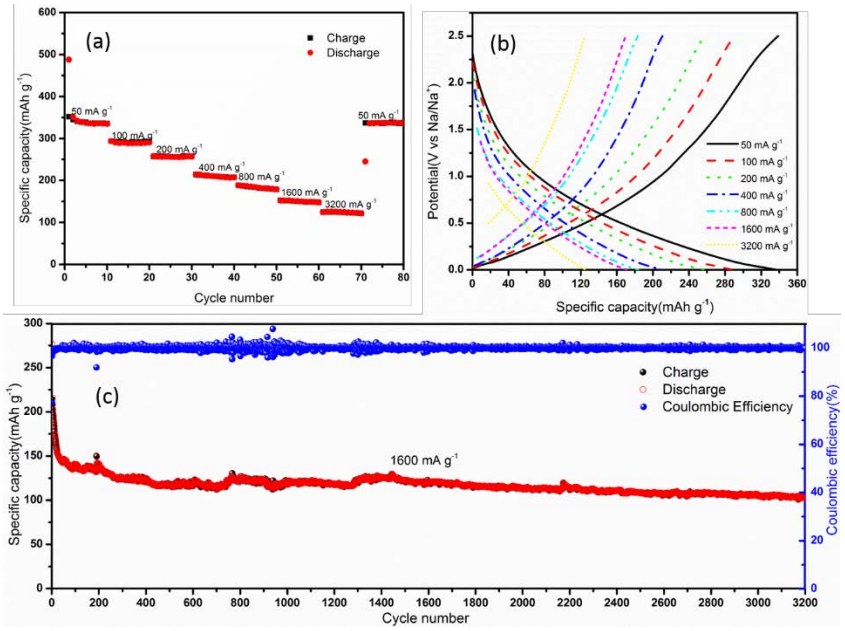

Fig.5 (a) Rate performance, (b) the corresponding discharging/charging curves at different current densities, (c) cycle performance and coulombic efficiency at 1600 mA g^{-1} for CBN35 carbon black.

In comparison, with EC/DEC-based electrolyte, the CBN35 carbon black only exhibits an initial reversible capacity of 127 mAh g^{-1} at 50 mA g^{-1} with 79.53% capacity retention after 100 cycles, as shown in Fig. s3. This is consistent with our previous results from distinct electrochemical properties for N330 carbon in different electrolyte. Moreover, CV measurement is employed to further understand the different electrochemical behaviors for CBN35 in different electrolytes. In EC/DEC-based electrolyte a strong peak around 0.5 V in first catholic process is observed, as illustrated in Fig. 6(a). This is attributed to the decomposition of electrolyte and uncontrolled formation of insulating solid electrolyte interphase (SEI) during the sodiation process. Interestingly, in DEGDME-based electrolyte only a small and broad peak can be found at around 0.5 V in first catholic reaction, signaling a weak, but noticeable, SEI formation process. It's widely recognized that a favorable SEI film would effectively inhibit the continuous decomposition of electrolyte at low potential and further stabilize the layered structure of graphite anode for long cycle life. This is especially important considering its structural

instability towards solvent co-intercalation for lithium ion batteries[89,90]. Nevertheless, the application of ether-based electrolyte in sodium systems with the controlled formation of thin SEI films seems to be more favorable for enabling high electrochemical activity and reversibility of porous carbon materials.[65] And the EIS results for discharged CBN35 electrodes in different electrolytes further confirm the underlying role of DEGDME solvent in performance promotion. In virtue of the as-obtained spectra, the SEI impedance between electrode and electrolyte relates to the horizontal axis intercept value in high frequency region while charge transfer resistance results in semicircle in medium frequency for discharged electrodes[81]. Compared to low resistance for discharged electrode in DEGDME-based electrolyte, the slightly increased SEI impedance and greatly increased charge transfer resistance in EC/DEC-based electrolyte clearly revealed the electrochemical and physiochemical undesirability for uncontrolled formation of thick SEI layer. This leads to a large amount of electrolyte consumption, as well as lowering the reversible capacity and coulombic efficiency, and hinders the efficient sodium ion transport for fast charging/discharging process.

In order to verify the aforementioned phenomena of the limited formation of SEI thin film with CBN35 carbon black electrodes, the surface sensitive TEY-mode C K-edge X-ray absorption spectra at different electrochemical states in DEGDME-based electrolyte are displayed in Fig.6(d). For pristine electrodes, sharp peaks at 285.4 eV and 292.4 eV can be found and are attributed to carbon 1s core electrons excited to π(C-C)* and σ(C-C)* orbitals[91] , respectively, while the small peak around 288.3 eV may be related to π (C=O)* transitions[91-94]. Following discharge to 0.001 V, a new peak appears around 290.1 eV that can be assigned to σ*(C-O) transitions for oxygen-containing functional groups[94-96] from electrolyte decomposition and SEI formation. Simultaneously, the π (C=O)* peak slightly shifts to high energy while peak intensities for both π(C-C)* and σ(C-C)* peaks decrease, further indicating the restrained formation of an SEI film during the discharging process. When charging the electrode back to 2.5 V, the σ*(C-O) peak can still be observed at 290.1 eV, but with low intensity, indicating a preserved SEI thin film. Therefore, the adoption of ether-based electrolyte in porous carbon could not only facilitate fast migration of sodium ions and solvated sodium ion species in electrolyte/interphase/electrode, but also efficiently enables the controlled SEI formation without sacrificing reversible capacity and electrolyte amount, leading to high electrochemical reversibility and cycle stability for CBN35.

Based on the analysis above, it appears that with assistance of ether-based electrolyte for the insertion of both sodium ion and solvated sodium ion, the intentionally designed porous carbon could deliver an exceptional reversible capacity with a prolonged cycle life. The improved performance results from the desirable formation of microporous structure with more sodium ion storage sites and controlled formation of SEI thin film for stabilizing the fragile porous structure and ensuring rapid sodium ions/ solvated sodium ion species transport. In addition to the suitable porosity, the heteroatom doping and surface functionalities can also affect the sodium ion storage capability of carbon-based materials. Such works are ongoing in our group.

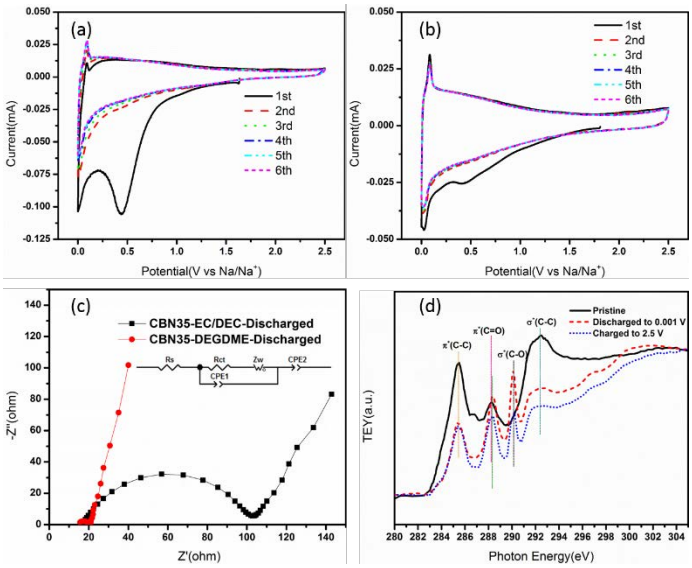

Fig. 6 CV curves of CBN35 carbon black in (a) EC/DEC-based and (b) DEGDME-based electrolytes. (c) Electrochemical impedance spectroscopy for discharged electrode in different electrolytes. (d) C K-edge X-ray absorption spectroscopy of CBN35 carbon black electrodes at different states when cycling in DEGDME-based electrolyte.

4. Conclusions

Porous carbon black was fabricated using a NH_3 etching method and has been successfully studied as an anode material for sodium-ion batteries with DEGDME-based electrolyte. The as-prepared CBN35 carbon black with highest microporosity and appropriate surface area delivers a large reversible capacity with superior rate capability and outstanding cycle stability. The improved sodium ion storage capability stems from the increased active sites in microporous structure, and the novel insertion mechanism of solvated sodium ion intercalation

into graphitic structure and sodium ion insertion into disordered structure. Moreover, the improved rate cycle stability is resulted from the controlled formation of a robust SEI thin film for structural stability and the consequent fast sodium ions/solvated sodium ion species migration. We believe this work on porous carbon in DEGDME-based electrolyte would enlighten a new strategy regarding rational structure design of carbon materials for high-performance sodium ion batteries in ether-based electrolyte.

Acknowledgements

This research was supported by the Natural Science and Engineering Research Council of Canada (NSERC), the Canada Research Chair Program (CRC), the Canada Foundation for Innovation (CFI), and the University of Western Ontario (UWO). Dr. Jian Liu is grateful to the financial support from NSERC Postdoctoral Fellowships Program. This research used resources of the Advanced Light Source, which is a DOE Office of Science User Facility under contract no. DE-AC02-05CH11231.

References

1 Armand, M. & Tarascon, J.-M. Building better batteries. *Nature* **451**, 652-657, doi:10.1038/451652a (2008).

2 Tarascon, J. M. Key challenges in future Li-battery research. *Phil. Trans. R. Soc. A* **368**, 3227-3241, doi:10.1098/rsta.2010.0112 (2010).

3 Tarascon, J.-M. & Armand, M. Issues and challenges facing rechargeable lithium batteries. *Nature*, 359-367, doi:doi:10.1038/35104644 (2001).

4 Ellis, B. L. & Nazar, L. F. Sodium and sodium-ion energy storage batteries. *Curr. Opin. Solid State Mater. Sci.* **16**, 168-177, doi:10.1016/j.cossms.2012.04.002 (2012).

5 Slater, M. D., Kim, D., Lee, E. & Johnson, C. S. Sodium-Ion Batteries. *Adv. Funct. Mater.* **23**, 947-958, doi:10.1002/adfm.201200691 (2013).

6 Palomares, V. *et al.* Na-ion batteries, recent advances and present challenges to become low cost energy storage systems. *Energy Environ. Sci.* **5**, 5884–5901, doi:10.1039/c2ee02781j (2012).

7 Pan, H., Hu, Y.-S. & Chen, L. Room-temperature stationary sodium-ion batteries for large-scale electric energy storage. *Energy Environ. Sci.* **6**, 2338, doi:10.1039/c3ee40847g (2013).

8 Yabuuchi, N., Kubota, K., Dahbi, M. & Komaba, S. Research development on sodium-ion batteries. *Chem. Rev.* **114**, 11636-11682, doi:10.1021/cr500192f (2014).

9 Kundu, D., Talaie, E., Duffort, V. & Nazar, L. F. The emerging chemistry of sodium ion batteries for electrochemical energy storage. *Angew. Chem. Int. Ed.* **54**, 3431-3448, doi:10.1002/anie.201410376 (2015).

10 Bommier, C. *et al.* New Paradigms on the Nature of Solid Electrolyte Interphase Formation and Capacity Fading of Hard Carbon Anodes in Na-Ion Batteries. *Adv. Mater. Interfaces* **3**, 1600449, doi:10.1002/admi.201600449 (2016).

11 Kim, Y., Ha, K. H., Oh, S. M. & Lee, K. T. High-capacity anode materials for sodium-ion batteries. *Chem. Eur. J.* **20**, 11980-11992, doi:10.1002/chem.201402511 (2014).

12 Hong, S. Y. *et al.* Charge carriers in rechargeable batteries: Na ions vs. Li ions. *Energy Environ. Sci.* **6**, 2067-2081, doi:10.1039/c3ee40811f (2013).

13 Doeff, M. M., Ma, Y., Visco, S. J. & Jonghe, L. C. D. Electrochemical Insertion of Sodium into Carbon. *J. Electrochem. Soc.* **140**, L169–L170, doi:10.1149/1.2221153 (1993).

14 Stevens, D. A. & Dahn, J. R. The Mechanisms of Lithium and Sodium Insertion in Carbon Materials. *J. Electrochem. Soc.* **148**, A803-A811, doi:10.1149/1.1379565 (2001).

15 Bommier, C., Surta, T. W., Dolgos, M. & Ji, X. New Mechanistic Insights on Na-Ion Storage in Nongraphitizable Carbon. *Nano Lett.* **15**, 5888-5892, doi:10.1021/acs.nanolett.5b01969 (2015).

16 Stevens, D. A. & Dahn, J. R. High Capacity Anode Materials for Rechargeable Sodium Ion Batteries. *J. Electrochem. Soc.* **147**, 1271-1273, doi:10.1149/1.1393348 (2000).

17 Thomas, P. & Billaud, D. Electrochemical insertion of sodium into hard carbons. *Electrochim. Acta* **47**, 3303-3307, doi:10.1016/S0013-4686(02)00250-5 (2002).

18 Alca´ntara, R. *et al.* Characterisation of mesocarbon microbeads (MCMB) as active electrode material in lithium and sodium cells. *Carbon* **38**, 1031–1041, doi:10.1016/S0008-6223(99)00215-8 (2001).

19 Alcántara, R., Jiménez Mateos, J. M. & Tirado, J. L. Negative Electrodes for Lithium- and Sodium-Ion Batteries Obtained by Heat-Treatment of Petroleum Cokes below 1000°C. *J. Electrochem. Soc.* **149**, A201-A205, doi:10.1149/1.1431963 (2002).

20 Alcántara, R., Jiménez-Mateos, J. M., Lavela, P. & Tirado, J. L. Carbon black-a promising electrode material for sodium-ion batteries. *Electrochem. Commun.* **3**, 639–642, doi:10.1016/S1388-2481(01)00244-2 (2001).

21 Alcántara, R., Lavela, P., Ortiz, G. F. & Tirado, J. L. Carbon Microspheres Obtained from Resorcinol-Formaldehyde as High-Capacity Electrodes for Sodium-Ion Batteries. *Electrochem. Solid-State Lett.* **8**, A222-A225, doi:10.1149/1.1870612 (2005).

22 Li, Y. *et al.* Advanced sodium-ion batteries using superior low cost pyrolyzed anthracite anode: towards practical applications. *Energy storage materials* **5**, 191-197, doi:10.1016/j.ensm.2016.07.006 (2016).

23 Li, H. *et al.* Carbonized-leaf Membrane with Anisotropic Surfaces for Sodium-ion Battery. *ACS applied materials & interfaces* **8**, 2204-2210, doi:10.1021/acsami.5b10875 (2016).

24 Liu, P. *et al.* A waste biomass derived hard carbon as a high-performance anode material for sodium-ion batteries. *J. Mater. Chem. A* **4**, 13046-13052, doi:10.1039/c6ta04877c (2016).

25 Aricò, A. S., Bruce, P., Scrosati, B., Tarascon, J.-M. & Schalkwijk, W. v. Nanostructured materials for advanced energy conversion and storage devices. *Nat. Mater.*, 366 - 377, doi:10.1038/nmat1368 (2005).

26 Bruce, P. G., Scrosati, B. & Tarascon, J. M. Nanomaterials for rechargeable lithium batteries. *Angew. Chem. Int. Ed. Engl.* **47**, 2930-2946, doi:10.1002/anie.200702505 (2008).

27 Wenzel, S., Hara, T., Janek, J. & Adelhelm, P. Room-temperature sodium-ion batteries: Improving the rate capability of carbon anode materials by templating strategies. *Energy Environ. Sci.* **4**, 3342–3345, doi:10.1039/c1ee01744f (2011).

28 Tang, K. *et al.* Hollow Carbon Nanospheres with Superior Rate Capability for Sodium-Based Batteries. *Adv. Energy. Mater.* **2**, 873-877, doi:10.1002/aenm.201100691 (2012).

29 Cao, Y. *et al.* Sodium ion insertion in hollow carbon nanowires for battery applications. *Nano Lett.* **12**, 3783-3787, doi:10.1021/nl3016957 (2012).

30 Yun, Y. S., Cho, S. Y., Kim, H., Jin, H.-J. & Kang, K. Ultra-Thin Hollow Carbon Nanospheres for Pseudocapacitive Sodium-Ion Storage. *ChemElectroChem* **2**, 359-365, doi:10.1002/celc.201402359 (2015).

31 Chen, T. *et al.* Electrospun carbon nanofibers as anode material for sodium ion batteries with excellent cycle performance. *J. Mater. Chem. A* **2**, 4117-4121, doi:10.1039/C3TA14806H (2014).

32 Jin, J., Shi, Z.-q. & Wang, C.-y. Electrochemical Performance of Electrospun carbon nanofibers as free-standing and binder-free anodes for Sodium-Ion and Lithium-Ion Batteries. *Electrochim. Acta* **141**, 302-310, doi:10.1016/j.electacta.2014.07.079 (2014).

33 Li, W. *et al.* Free-standing and binder-free sodium-ion electrodes with ultralong cycle life and high rate performance based on porous carbon nanofibers. *Nanoscale* **6**, 693-698, doi:10.1039/c3nr05022j (2014).

34 Luo, W. *et al.* Carbon nanofibers derived from cellulose nanofibers as a long-life anode material for rechargeable sodium-ion batteries. *J. Mater. Chem. A* **1**, 10662–10666, doi:10.1039/c3ta12389h (2013).

35 Zhao, P.-Y., Zhang, J., Li, Q. & Wang, C.-Y. Electrochemical performance of fulvic acid-based electrospun hard carbon nanofibers as promising anodes for sodium-ion batteries. *J. Power Sources* **334**, 170-178, doi:10.1016/j.jpowsour.2016.10.029 (2016).

36 Li, Y., Hu, Y.-S., Titirici, M.-M., Chen, L. & Huang, X. Hard Carbon Microtubes Made from Renewable Cotton as High-Performance Anode Material for Sodium-Ion Batteries. *Adv. Energy Mater.*, 1600659, doi:10.1002/aenm.201600659 (2016).

37 Wang, Y.-X., Chou, S.-L., Liu, H.-K. & Dou, S.-X. Reduced graphene oxide with superior cycling stability and rate capability for sodium storage. *Carbon* **57**, 202-208, doi:10.1016/j.carbon.2013.01.064 (2013).

38 Luo, X.-F. *et al.* Microplasma-assisted bottom-up synthesis of graphene nanosheets with superior sodium-ion storage performance. *J. Mater. Chem. A* **4**, 7624–7631, doi:10.1039/c6ta00743k (2016).

39 Wang, Y., Wang, C., Wang, Y., Liu, H. & Huang, Z. Boric Acid Assisted Reduction of Graphene Oxide: A Promising Material for Sodium-Ion Batteries. *ACS Appl. Mater. Interfaces* **8**, 18860-18866, doi:10.1021/acsami.6b04774 (2016).

40 Yang, J., Zhou, X., Wu, D., Zhao, X. & Zhou, Z. S-Doped N-Rich Carbon Nanosheets with Expanded Interlayer Distance as Anode Materials for Sodium-Ion Batteries. *Adv. Mater.* **29**, doi:10.1002/adma.201604108 (2017).

41 Ding, J. *et al.* Carbon Nanosheet Frameworks Derived from Peat Moss as High Performance Sodium Ion Battery Anodes. *ACS Nano* **7**, 11004–11015, doi:10.1021/nn404640c (2013).

42 Hou, H., Banks, C. E., Jing, M., Zhang, Y. & Ji, X. Carbon Quantum Dots and Their Derivative 3D Porous Carbon Frameworks for Sodium-Ion Batteries with Ultralong Cycle Life. *Adv. Mater.* **27**, 7861–7866, doi:10.1002/adma.201503816 (2015).

43 Wang, M., Yang, Z., Li, W., Gu, L. & Yu, Y. Superior Sodium Storage in 3D Interconnected Nitrogen and Oxygen Dual-Doped Carbon Network. *Small* **12**, 2529, doi:10.1002/smll.201600101 (2016).

44 Yuan, Z., Si, L. & Zhu, X. Three-dimensional hard carbon matrix for sodium-ion battery anode with superior-rate performance and ultralong cycle life. *J. Mater. Chem. A* **3**, 23403-23411, doi:10.1039/c5ta07223a (2015).

45 Fu, L. *et al.* Nitrogen doped porous carbon fibres as anode materials for sodium ion batteries with excellent rate performance. *Nanoscale* **6**, 1384-1389, doi:10.1039/c3nr05374a (2014).

46 Li, D. *et al.* Nitrogen-doped bamboo-like carbon nanotubes: promising anode materials for sodium-ion batteries. *Chem. Commun.* **51**, 16045-16048, doi:10.1039/C5CC06266G (2015).

47 Xu, J. *et al.* High-Performance Sodium Ion Batteries Based on Three-Dimensional Anode from Nitrogen-Doped Graphene Foams. *Adv. Mater.* **27**, 2042-2048, doi:10.1002/adma.201405370 (2015).

48 Yang, F. *et al.* Dopamine derived nitrogen-doped carbon sheets as anode materials for high-performance sodium ion batteries. *Carbon* **91**, 88-95, doi:10.1016/j.carbon.2015.04.049 (2015).
49 Zhang, K. *et al.* Nitrogen-doped porous interconnected double-shelled hollow carbon spheres with high capacity for lithium ion batteries and sodium ion batteries. *Electrochim. Acta* **155**, 174-182, doi:10.1016/j.electacta.2014.12.108 (2015).
50 Liu, H. *et al.* Nitrogen-doped carbon/graphene hybrid anode material for sodium-ion batteries with excellent rate capability. *J. Power Sources* **319**, 195-201, doi:10.1016/j.jpowsour.2016.04.040 (2016).
51 Yan, D. *et al.* Nitrogen-doped carbon microspheres derived from oatmeal as high capacity and superior long life anode material for sodium ion battery. *Electrochem. Acta* **191**, 385-391, doi:10.1016/j.electacta.2016.01.105 (2016).
52 Li, W. *et al.* A high performance sulfur-doped disordered carbon anode for sodium ion batteries. *Energy Environ. Sci.* **8**, 2916-2921, doi:10.1039/c5ee01985k (2015).
53 Zhang, S., Yao, F., Yang, L., Zhang, F. & Xu, S. Sulfur-doped mesoporous carbon from surfactant-intercalated layered double hydroxide precursor as high-performance anode nanomaterials for both Li-ion and Na-ion batteries. *Carbon* **93**, 143-150, doi:10.1016/j.carbon.2015.04.091 (2015).
54 Wang, X. *et al.* Sulfur covalently bonded graphene with large capacity and high rate for high-performance sodium-ion batteries anodes. *Nano Energy* **15**, 746-754, doi:10.1016/j.nanoen.2015.05.038 (2015).
55 Wang, P. *et al.* Fluorine-Doped Carbon Particles Derived from Lotus Petioles as High-Performance Anode Materials for Sodium-Ion Batteries. *J. Phys. Chem. C* **119**, 21336-21344, doi:10.1021/acs.jpcc.5b05443 (2015).
56 Yoon, D. *et al.* Hydrogen-enriched porous carbon nanosheets with high sodium storage capacity. *Carbon* **98**, 213-220, doi:10.1016/j.carbon.2015.11.009 (2016).
57 Li, Z. *et al.* High Capacity of Hard Carbon Anode in Na-Ion Batteries Unlocked by POx Doping. *ACS Energy Lett.* **1**, 395-401, doi:10.1021/acsenergylett.6b00172 (2016).
58 Lv, W. *et al.* Carbonaceous photonic crystals as ultralong cycling anodes for lithium and sodium batteries. *J. Mater. Chem. A* **3**, 13786-13793, doi:10.1039/C5TA02873F (2015).
59 Hong, K.-l. *et al.* Biomass derived hard carbon used as a high performance anode material for sodium ion batteries. *J. Mater. Chem. A* **2**, 12733-12738, doi:10.1039/c4ta02068e (2014).
60 Li, Y. *et al.* Amorphous monodispersed hard carbon micro-spherules derived from biomass as a high performance negative electrode material for sodium-ion batteries. *J. Mater. Chem. A* **3**, 71-77, doi:10.1039/c4ta05451b (2014).
61 Gaddam, R. R. *et al.* Biomass derived carbon nanoparticle as anodes for high performance sodium and lithium ion batteries. *Nano Energy* **26**, 346-352, doi:10.1016/j.nanoen.2016.05.047 (2016).
62 Jache, B. & Adelhelm, P. Use of Graphite as a Highly Reversible Electrode with Superior Cycle Life for Sodium-Ion Batteries by Making Use of Co-Intercalation Phenomena. *Angew. Chem.* **53**, 10169-10173, doi:10.1002/anie.201403734 (2014).
63 Kim, H. *et al.* Sodium Storage Behavior in Natural Graphite using Ether-based Electrolyte Systems. *Adv. Funct. Mater.* **25**, 534-541, doi:10.1002/adfm.201402984 (2014).
64 Kim, H. *et al.* Sodium intercalation chemistry in graphite. *Energy Environ. Sci.* **8**, 2963-2969, doi:10.1039/c5ee02051d (2015).
65 Zhang, J. *et al.* Achieving superb sodium storage performance on carbon anodes through an ether-derived solid electrolyte interphase. *Energy Environ. Sci.* **10**, 370, doi:10.1039/c6ee03367a (2017).
66 Li, Y. *et al.* Carbon black cathodes for lithium oxygen batteries: Influence of porosity and heteroatom-doping. *Carbon* **64**, 170-177, doi:10.1016/j.carbon.2013.07.049 (2013).

67 Li, Y., Hu, Y.-S., Li, H., Chen, L. & Huang, X. A superior low-cost amorphous carbon anode made from pitch and lignin for sodium-ion batteries. *J. Mater. Chem. A*, doi:10.1039/C5TA08601A (2015).

68 Biscoe, J. An X-Ray Study of Carbon Black. *J. Appl. Phys.* **13**, 364, doi:10.1063/1.1714879 (1942).

69 Jaouen, F. & Dodelet, J.-P. Non-Noble Electrocatalysts for O_2 Reduction: How Does Heat Treatment Affect Their Activity and Structure? Part I. Model for Carbon Black Gasification by NH_3: Parametric Calibration and Electrochemical Validation. *J. Phys. Chem. C* **111**, 5963-5970, doi:10.1021/jp068273p (2007).

70 Jaouen, F., Serventi, A. M., Lefevre, M., Dodelet, J.-P. & Bertrand, P. Non-Noble Electrocatalysts for O_2 Reduction: How Does Heat Treatment Affect Their Activity and Structure? Part II. Structural Changes Observed by Electron Microscopy, Raman, and Mass Spectroscopy. *J. Phys. Chem. C* **111**, 5971-5976 (2007).

71 Li, Y. *et al.* Pitch-derived amorphous carbon as high performance anode for sodium-ion batteries. *Energy storage materials* **2**, 139-145, doi:10.1016/j.ensm.2015.10.003i (2016).

72 Chai, L. *et al.* Porous carbonized graphene-embedded fungus film as an interlayer for superior Li–S batteries. *Nano Energy* **17**, 224-232, doi:10.1016/j.nanoen.2015.09.001 (2015).

73 Haerle, R., Riedo, E., Pasquarello, A. & Baldereschi, A. sp2/sp3 hybridization ratio in amorphous carbon from C1score-level shifts: X-ray photoelectron spectroscopy and first-principles calculation. *Phys. Rev. B* **65**, doi:10.1103/PhysRevB.65.045101 (2001).

74 Merel, P., Tabbal, M., Chaker, M., Moisa, S. & Margot, J. Direct evaluation of the sp3 content in diamond-like-carbon films by XPS. *Appl. Surf. Sci.* **136**, 105–110 (1998).

75 Morant, C. *et al.* XPS characterization of nitrogen-doped carbon nanotubes. *phys. status solidi (a)* **203**, 1069-1075, doi:10.1002/pssa.200566110 (2006).

76 Chan, L. H. *et al.* Resolution of the binding configuration in nitrogen-doped carbon nanotubes. *Phys. Rev. B* **70**, doi:10.1103/PhysRevB.70.125408 (2004).

77 Jia, R. *et al.* Synthesis of highly nitrogen-doped hollow carbon nanoparticles and their excellent electrocatalytic properties in dye-sensitized solar cells. *J. Mater. Chem.* **20**, 10829, doi:10.1039/c0jm01799j (2010).

78 Yan, X., Xu, T., Chen, G., Yang, S. & Liu, H. Study of structure, tribological properties and growth mechanism of DLC and nitrogen-doped DLC films deposited by electrochemical technique. *Appl. Surf. Sci.* **236**, 328-335, doi:10.1016/j.apsusc.2004.05.005 (2004).

79 Yan, J. *et al.* Electrochemical properties of graphene nanosheet/carbon black composites as electrodes for supercapacitors. *Carbon* **48**, 1731-1737, doi:10.1016/j.carbon.2010.01.014 (2010).

80 Yang, S.-Y. *et al.* Design and tailoring of a hierarchical graphene-carbon nanotube architecture for supercapacitors. *J. Mater. Chem.* **21**, 2374-2380, doi:10.1039/c0jm03199b (2011).

81 Xiao, L. *et al.* Hard Carbon Nanoparticles as High-capacity, High-stability Anodic Materials for Na-ion Batteries. *Nano Energy*, doi:10.1016/j.nanoen.2015.10.034 (2015).

82 Li, S. *et al.* Surface capacitive contributions: Towards high rate anode materials for sodium ion batteries. *Nano Energy* **12**, 224–230, doi:10.1016/j.nanoen.2014.12.032 (2015).

83 Bai, Y. *et al.* Hard carbon originated from polyvinyl chloride nanofibers as high performance anode material for Na-ion battery. *ACS Appl. Mater. Interfaces* **7**, 5598-5604, doi:10.1021/acsami.5b00861 (2015).

84 Yang, G., Song, H., Cuiab, H. & Wang, C. Honeycomb in honeycomb carbon bubbles- excellent Li- and Na-storage performances. *J. Mater. Chem. A* **3**, 20065–20072, doi:10.1039/c5ta04561d (2015).

85 Jo, C., Park, Y., Jeong, J., Lee, K. T. & Lee, J. Structural Effect on Electrochemical Performance of Ordered Porous Carbon Electrodes for Na-Ion Batteries. *ACS Appl. Mater. Interfaces* **7**, 11748-11754, doi:10.1021/acsami.5b03186 (2015).
86 Licht, S. *et al.* Carbon Nanotubes Produced from Ambient Carbon Dioxide for Environmentally Sustainable Lithium-Ion and Sodium-Ion Battery Anodes. *ACS Cent. Sci.* **2**, 162-168, doi:10.1021/acscentsci.5b00400 (2016).
87 Wen, Y., Wang, B., Luo, B. & Wang, L. Long-Term Cycling Performance of Nitrogen-Doped Hollow Carbon Nanospheres as Anode Materials for Sodium-Ion Batteries. *Eur. J. Inorg. Chem.* **2016**, 2051-2055, doi:10.1002/ejic.201501172 (2016).
88 Deng, X. *et al.* Scalable synthesis of self-standing sulfur-doped flexible graphene films as recyclable anode materials for low-cost sodium-ion batteries. *Carbon* **107**, 67-73, doi:10.1016/j.carbon.2016.05.052 (2016).
89 Peled, E. The Electrochemical Behavior of Alkali and Alkaline Earth Metals in Nonaqueous Battery Systems-The Solid Electrolyte Interphase Model. *J. Electrochem. Soc.* **126**, 2047-2051, doi:10.1149/1.2128859 (1973).
90 Xu, K. Electrolytes and interphases in Li-ion batteries and beyond. *Chem. Rev.* **114**, 11503-11618, doi:10.1021/cr500003w (2014).
91 Zhou, J. *et al.* Electronic structure and luminescence center of blue luminescent carbon nanocrystals. *Chem. Phys. Lett.* **474**, 320-324, doi:10.1016/j.cplett.2009.04.075 (2009).
92 Zhou, J. *et al.* Interaction between Pt nanoparticles and carbon nanotubes – An X-ray absorption near edge structures (XANES) study. *Chem. Phys. Lett.* **437**, 229-232, doi:10.1016/j.cplett.2007.02.026 (2007).
93 Bouchet-Fabre, B. *et al.* NEXAFS and X-ray scattering study of structure changes after post-annealing treatments of aligned MWNTs. *Diamond Relat. Mater.* **14**, 881-886, doi:10.1016/j.diamond.2004.11.018 (2005).
94 Roy, S. S., Papakonstantinou, P., Okpalugo, T. I. T. & Murphy, H. Temperature dependent evolution of the local electronic structure of atmospheric plasma treated carbon nanotubes: Near edge x-ray absorption fine structure study. *J. Appl. Phys.* **100**, 053703, doi:10.1063/1.2260821 (2006).
95 Banerjee, S. *et al.* Ozonized single-walled carbon nanotubes investigated using NEXAFS spectroscopy. *Chem. Commun.*, 772-773, doi:10.1039/b315390h (2004).
96 Kuznetsova, A. *et al.* Oxygen-Containing Functional Groups on Single-Wall Carbon Nanotubes: NEXAFS and Vibrational Spectroscopic Studies. *J. Am. Chem. Soc.* **123**, 10699–10704 (2001).